THE JOURNAL OF PHYSICAL CHEMISTRY Letters

pubs.acs.org/JPCL Letter

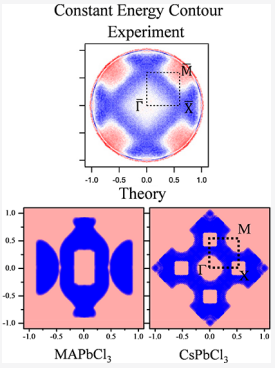
Probing the Electronic Structure of Hybrid Perovskites in the Orientationally Disordered Cubic Phase

Pronoy Nandi,[▽] S. K. Pandey,[▽] Chandan Giri, Vijay Singh, L. Petaccia, U. Manju, Subhendra D. Mahanti, and D. Topwal*

Cite This: *J. Phys. Chem. Lett.* 2020, 11, 5719–5727 Read Online

ACCESS | Metrics & More | Article Recommendations | Supporting Information

ABSTRACT: Hybrid organic–inorganic lead halide perovskites are projected as new generation photovoltaic and optoelectronic materials with improved efficiencies. However, their electronic structure so far remains poorly understood, particularly in the orientationally disordered cubic phase. We performed electronic structure investigations using angle-resolved photoemission spectroscopy on two prototypical samples ($MAPbBr_3$ and $MAPbCl_3$) in their cubic phase, and the results are compared with the calculations within two theoretical models where MA^+ is orientationally (1) disordered (MA^+ ion is replaced by spherically symmetric Cs^+ ion) and (2) ordered (MA oriented along (100) direction) but keeping the symmetry of the unit cell cubic. Degeneracy of the valence bands and behavior of constant energy contours are consistent with model 1, which supports strongly the disordered nature of the orientation of the MA^+ ions in the cubic phase. Band structure calculations also reveal that spin–orbit coupling induced Rashba splitting is suppressed by the orientational disorder.



Downloaded via PEKING UNIV on September 16, 2024 at 10:21:41 (UTC).
See https://pubs.acs.org/sharingguidelines for options on how to legitimately share published articles.

Organic–inorganic halide perovskites of the type $MAPbX_3$ ($MA = CH_3NH_3$, i.e., methylammonium and X = Cl, Br, and I) are one of the most widely investigated classes of systems for photovoltaic applications due to their strong light absorption ability[1] coupled with the ease and low cost of fabrication.[2] Further, their excellent performance in a solar cell, with above 25% efficiency,[3] almost at the level of commercially available silicon cells, has stimulated considerable interest to understand the photophysical properties of these systems.[4,5] However, fundamental questions concerning their electronic structure, importance of spin–orbit coupling, and the effect of orientational disorder (of methylammonium) on their electronic structures are not well understood.[6−15]

It is known that the organic cations MA^+ do not contribute directly to the electronic states near either the highest valence or the lowest conduction bands, which contribute predominantly to the charge carriers. However, their orientation in the crystal strongly influences the optoelectronic properties.[13−15] Changing MA^+ orientation from (100) to (111) direction has a profound effect on the electronic structure, namely, the bandgap changes from direct to indirect.[15] Further, it is observed that the orientational dynamics of the MA^+ ion inside the PbX_6 octahedral cage is responsible for strong frequency dependence of the relative permittivity,[16] reduction of the Fröhlich electron–phonon coupling[17] and reduction in the thermal stability of the hybrid perovskites.[18]

Electronic band structure of hybrid perovskites were also found to be sensitive to the orientation of the MA^+ ions, the choice of exchange–correlation functional,[19,20] and relativistic effects, i.e., spin–orbit coupling (SOC).[20] One of the earlier studies predict Rashba spin-split bands for specific orientation of the MA^+ ions.[21] However, some of these theoretical findings are in disagreement with experimental observations. For example, angle-resolved photoemission spectroscopy (ARPES) study by Komesu et al.[11] reported the absence of any *k*-dependent spin-splitting of the bands in their room temperature experiments, (where the MA^+ ions are orientationally disordered) whereas another experimental study by Niesner et al.[12] suggested giant splitting of ∼0.086 $Å^{-1}$ in the same high temperature cubic phase of $MAPbBr_3$. The precise nature of the Rashba spin-split states from experimental and theoretical investigations is also controversial. Niesner et al.[12] suggested the presence of Rashba spin-split bands near the valence band maxima, i.e., near the $\bar{M}$ point in the cubic phase and also in the low temperature orthorhombic phase, whereas theoretical calculations based on density functional theory (DFT) did not find any such spin-splitting near the $\bar{M}$ point, rather a small spin splitting was found near the $\bar{\Gamma}$ point.[22]

In this work, we revisit the issues mentioned above and discuss the electronic structure of $MAPbCl_3$ and $MAPbBr_3$ single crystals in the cubic phase using photoelectron spectroscopy (angle-integrated and angle-resolved) along with first-principles band structure calculations based on

Received: May 6, 2020
Accepted: July 1, 2020
Published: July 1, 2020



© 2020 American Chemical Society

https://dx.doi.org/10.1021/acs.jpclett.0c01386
J. Phys. Chem. Lett. 2020, 11, 5719–5727

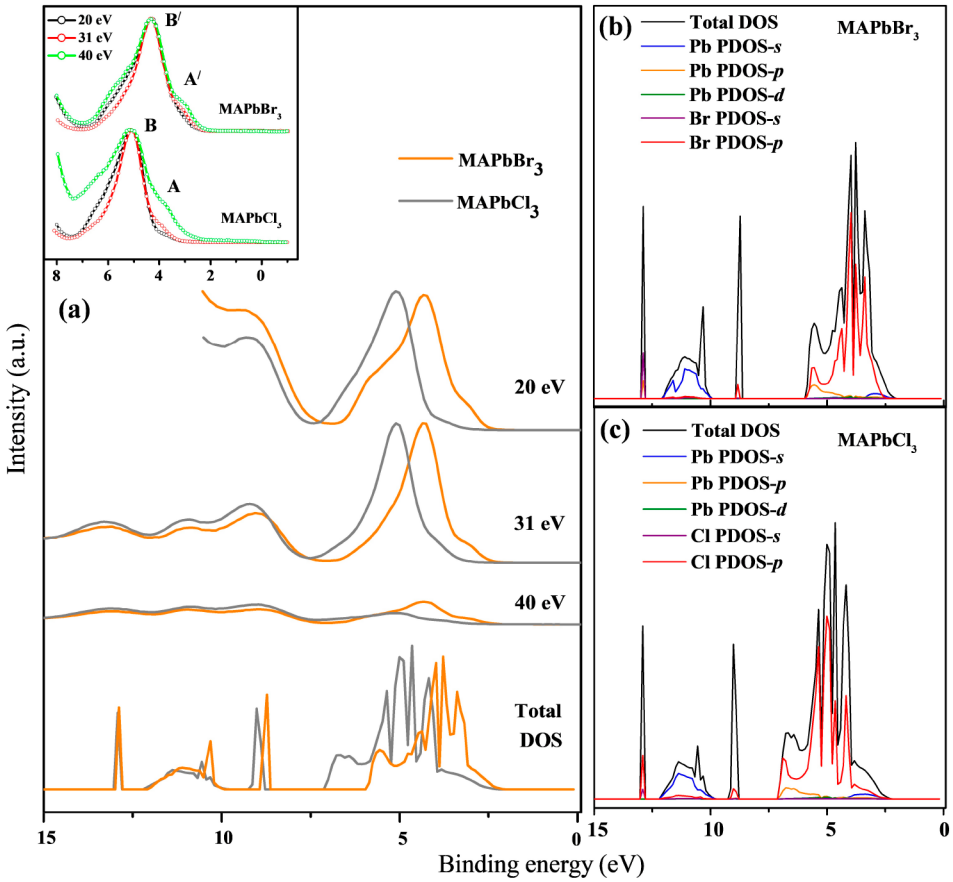


Figure 1. (a) Experimental angle-integrated valence band spectra acquired at 20, 31, and 40 eV photon energies in comparison to the calculated total DOS for $MAPbBr_3$ and $MAPbCl_3$ using model 2 where the molecules are oriented along the (100) axis but keep the unit cell cubic. The inset to the figure shows all valence band spectra (with different photon energies) normalized and plotted in the same figure for comparison. Calculated total and orbital projected density of states for (b) $MAPbBr_3$ and (c) $MAPbCl_3$. The delta-function peaks between 9 and 13 eV come from the C and N atoms of the MA^+ molecule.

density functional theory using different models to handle orientational order/disorder of MA^+ ions. To theoretically investigate the effect of orientational disorder on the electronic band structure properly in a molecular solid using *ab-inito* methods is indeed a very difficult problem. If we assume that the molecular orientational dynamics time scales are similar to phonon time scales, then the electrons essentially propagate in a disordered medium. If the electronic states of interest consist of orbitals associated with the molecule itself as in M_3C_{60} solids[23] and MO_2[24−26] (M is an alkali atom), then methods like coherent potential approximation (CPA) and cluster CPA are needed.[23] If, however, the orbitals of interest belong to atoms other than the molecular species as in $MAPbCl_3$ and $MAPbBr_3$, then one can avoid using CPA or similar methods and use simpler approaches as discussed below.

Consider the potential produced by MA^+ ion seen by an electron inside a unit cell. In general, it will be nonspherical and can be written as (we have chosen the center of the molecule as the origin)

$$V_{MA^+}(\vec{r}) = V_s(r) + V_{ns}(\vec{r};\hat{\Omega})$$

The spherical part $V_s(r)$ does not depend on the orientation of the MA^+ ion $\hat{\Omega}$, whereas the nonspherical part $V_{ns}(\vec{r};\hat{\Omega})$ does. The spherical average of $V_{ns}(\vec{r};\hat{\Omega})$ over the molecular orientations $\hat{\Omega}$ is $\langle V_{ns}(\vec{r};\hat{\Omega})\rangle_{\hat{\Omega}} = 0$. If the molecular orientational dynamics were fast compared to the electronic time scale, then $V_s(r)$ will control the band structure. If not, then one has to treat the orientational disorder carefully using CPA-like methods. Instead, we use two different extreme models for band structure calculations considering the following assumptions. (i) The nonspherical part is small and can be neglected, particularly for the states arising from Pb-s and X-p orbitals. To obtain the spherical part, we replace MA^+ ion by Cs^+ ion, referred to as model 1 in the following text. (Optimization of lattice parameters and related information are provided in Supporting Information.) (ii) All the MA^+ molecules are oriented in the same direction (along (100) direction) but keep the unit cell cubic (average global structure in the disordered phase); this model gives a measure of the strength of the nonspherical part of the potential and its effect on the band structure. It is referred as model 2. As pointed out by Sarkar et al.,[14] there are subtle effects on the band structure of $MAPbBr_3$ at low temperature where the MA^+ molecules are orientationally ordered and the lattice is noncubic. Recently, Mannino et al.[27] and Zhu et al.[28] carried out a comparative study of band edge carrier dynamics in $MAPbBr_3$, $FAPbBr_3$, and $CsPbBr_3$ and showed how orientational disorder of organic cation affects the band edge parameters (bandgap, absorption coefficient, recombination rate constant, *etc.*). However, no explicit proposal was presented about how to treat the effect of orientational disorder of the MA molecule and how and under what conditions it could be approximated in the zeroth order by replacing the molecule by a Cs atom. We believe such an

https://dx.doi.org/10.1021/acs.jpclett.0c01386
J. Phys. Chem. Lett. 2020, 11, 5719−5727

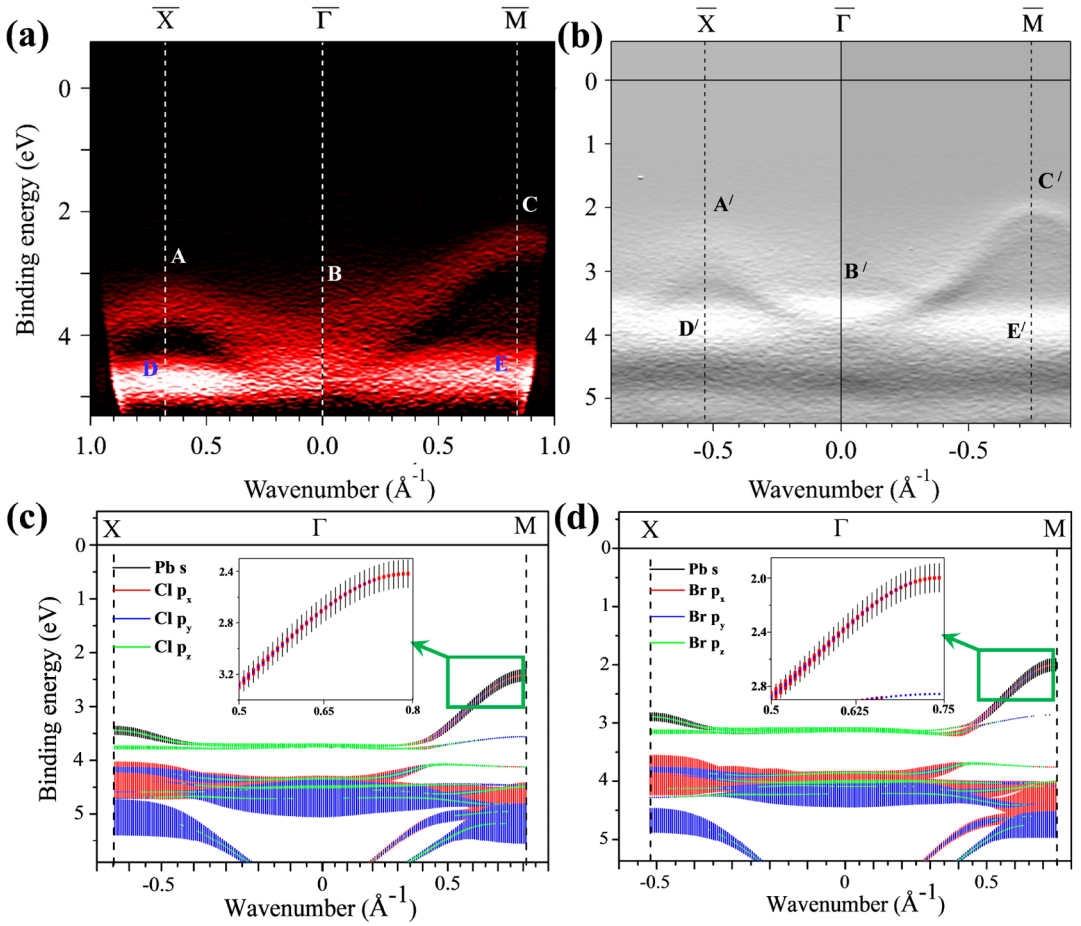


Figure 2. Valence band structure of $MAPbCl_3$ [(a) and (c)] and $MAPbBr_3$[(b) and (d)]. Experimental band dispersion obtained from angle-resolved photoemission spectroscopy (ARPES), acquired at a photon energy of 37 eV [(a), (b)]. Calculated band structure [(c), (d)] using model 2 (see text).

approximation will help in understanding the strongly disordered nature of the orientation of the MA^+ ions in the cubic phase.

Angle-integrated photoemission spectra of $MAPbBr_3$ and $MAPbCl_3$, acquired with different photon energies are depicted in Figure 1a. Valence band edges of these two compounds were extracted by extrapolating the experimental spectra with the baseline and the intersects are observed at binding energies of 2.16 and 2.48 eV for $MAPbBr_3$ and $MAPbCl_3$, respectively, with the top of the valence band for $MAPbCl_3$ approximately 0.32 eV higher in energy than $MAPbBr_3$, in good agreement with the earlier reports.[7,13] Additionally, it is also observed that the entire valence band spectrum, including the features between 8 and 10 eV, for $MAPbCl_3$ are shifted to higher binding energies for all acquired photon energies. The calculated total DOS of both the compounds for model 2 are also presented in the bottom part of Figure 1a. Ignoring the sharp nearly delta-function-like peaks associated with the molecular states of MA^+, and considering only the lead halide contributions to the experimental spectra, we analyzed the atom projected density of states (PDOS) for Pb, Br, and Cl atomic orbitals and results are presented in Figure 1b,c, respectively. From the PDOS calculations, it is evident that, though the Pb spectral weight contibutes throughout the top of the valence band,[29] both the halide and Pb PDOS are shifted toward higher binding energies for the $MAPbCl_3$ perovskite, which is consistent with our experimental results. Different electron affinities and the chemical bonding of halide ions are responsible for this binding energy shift.[13]

To gain further insight into the orbitals involved in hybridization, normalized photoemitted intensity of the ejected electrons (density of states) was compared using different photon energies, as shown in the inset of Figure 1a. Based on the photoionization cross-section analysis (Table S2), our results suggest that the Pb-s state has a significant contribution near the valence band edge, i.e., at A and A′, whereas the halogen p states make dominant contributions at B and B′. PDOS calculations also support the experimental findings; they reveal that the major contributions to the valence band arise from the Cl-3p or Br-4p orbitals, while a substantial contribution from Pb-6s orbitals is present both at the top of the valence band and well below 9 eV from the Fermi level. This can be understood in terms of bonding−antibonding levels resulting from Pb-6s−Br/Cl-p hybridization.[29] The bonding levels are deep below the Fermi level (at ∼9 eV binding energy) and have dominantly Pb-s character, while the antibonding levels are close to the Fermi energy with predominantly Br/Cl-p character. Different aspects of this hybridization will be discussed in detail in the following sections.

ARPES measurements were performed at room temperature on the (001) grown surface of the crystals, as revealed by X-ray diffraction pattern (XRD) (Figure S1d). The experimental results are plotted along $\bar{\Gamma}-\bar{X}$ and $\bar{\Gamma}-\bar{M}$ symmetry directions

https://dx.doi.org/10.1021/acs.jpclett.0c01386
J. Phys. Chem. Lett. 2020, 11, 5719−5727

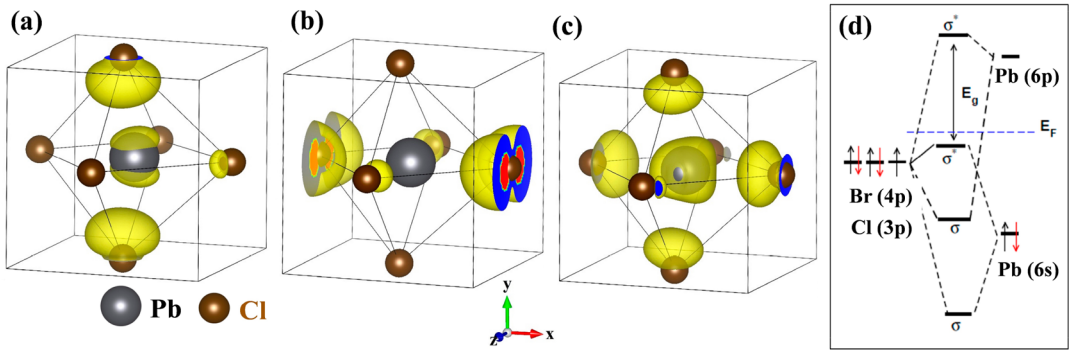


Figure 3. Charge density plot of $MAPbCl_3$ for the valence band maximum at (a) the $\bar{X}$ point, (b) the $\bar{\Gamma}$ point, and (c) the $\bar{M}$ point. (d) Schematic representation of sp hybridization in hybrid perovskites.

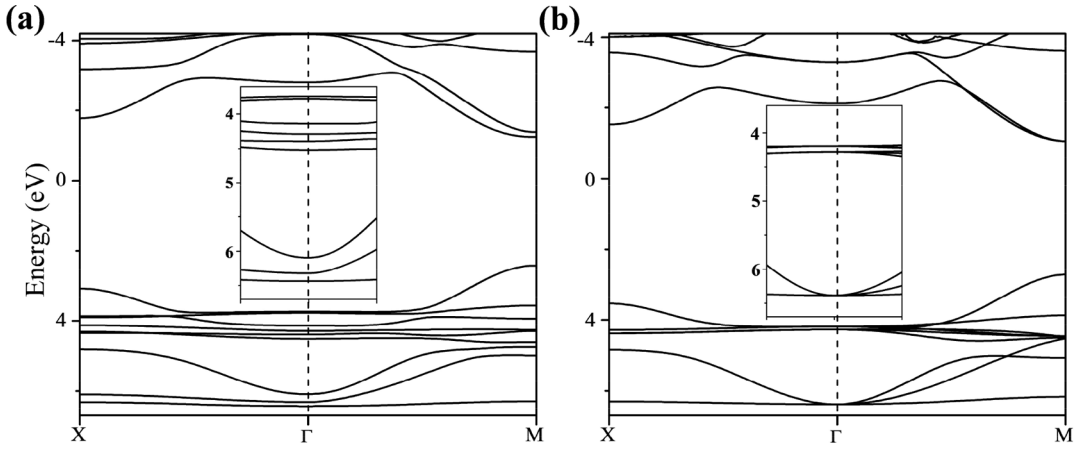


Figure 4. Calculated band structure of (a) $MAPbCl_3$ (model 2) and (b) $CsPbCl_3$ (model 1). The inset shows the zoomed view near the Γ point.

of the surface Brillouin zone (Figure S1e). Panels a and b of Figure 2 display the first derivative of ARPES intensity map along $\bar{X}-\bar{\Gamma}-\bar{M}$ symmetry directions for $MAPbCl_3$ and $MAPbBr_3$ crystals, respectively. A strongly dispersing downward band around $\bar{X}$ and $\bar{M}$ symmetry points with dispersion reaching a minimum at $\bar{\Gamma}$ is observed. The absence of any spectral density between E_F (zero of energy scale) and above the top of the stated bands suggests that the maximum of the valence band projected onto the (001) plane lies at a binding energy of 2.4 eV (2.1 eV) at the $\bar{M}$ point (denoted by C (C′)), while the band peaks at 3.1 eV (2.4 eV) at the $\bar{X}$ point (denoted by A (A′)) for $MAPbCl_3$ ($MAPbBr_3$). Large weakly dispersing spectral weight is observed around 4.6 eV (4.1 eV) at the zone center ($\bar{\Gamma}$ point, (denoted by B (B′))) and below 4.2 eV (3.6 eV) at the two zone edges ($\bar{X}$ and $\bar{M}$ point) of $MAPbCl_3$ ($MAPbBr_3$), which are denoted by D−E (D′−E′) in Figure 2a,b, respectively. Noticeably, for the parallel component of the surface momentum ($k_{||}$), the $\bar{X}$ point is at 0.67 $Å^{-1}$ (0.53 $Å^{-1}$) and the $\bar{M}$ point is at 0.83 $Å^{-1}$ (0.75 $Å^{-1}$) for $MAPbCl_3$ ($MAPbBr_3$), which are in good agreement with the values calculated from lattice parameters.[7,11,12]

To gain insight into the orbital character of the bands, DFT calculated bulk band structure for $MAPbCl_3$ and $MAPbBr_3$ using model 2 where the MA^+ ions are ordered parallel to each other (ferro-ordered) along the (100) direction, but constraining the unit cell to be cubic, were analyzed and are depicted in Figure 2c,d, respectively, with fat band representation for Pb-s and halide-p orbitals. For the highest occupied valence bands at the X, M, and Γ points, it is observed that the bands at the X point have contributions from the Pb-s orbital and Cl/Br-p orbitals. The same set of orbitals also contribute to the valence band maximum at M with the difference that at X only the Cl/Br-p_y has substantial contributions while at M both p_y and p_x orbitals contribute equally to the valence band maximum. However, the highest occupied band at Γ has mostly Cl/Br-p_z character.

This analysis also highlights the nature of Pb−Cl/Br covalency, which can be understood by calculating the charge densities at X, Γ, and M for the highest occupied bands, depicted in Figure 3 for $MAPbCl_3$. In Figure 3a, the charge density at X plotted for the valence band maximum clearly suggests that Pb-s and Cl-p_y orbitals are contributing to the valence band maximum while the contribution from other Cl-p orbitals are minimal/absent. At Γ (Figure 3b), only the Cl-p_z orbital contributes and no s−p (Pb−Cl) hybridization is observed. Further, at M (Figure 3c), the valence band maximum has contributions from Pb-s as well as Cl-p_x and p_y orbitals. This characteristic contribution of the halide p orbitals at various high symmetry points in the Brillouin zone (BZ) can be understood from the symmetry analysis of a tight-binding Hamiltonian.[30] An average over all possible orientation of organic cations at high temperature restores the full cubic symmetry. Contributions from the different Cl/Br-p orbitals at different *k*-points appear by symmetry allowed hopping between Pb-s and Cl/Br-p orbitals. At the X (0, 0.5, 0) (M (0.5, 0.5, 0.0)) point, the phase of the Bloch states allows the mixing of Pb-s and Cl/Br-p_y (p_xp_y). Hence their corresponding orbital character at these *k*-points shows up at the VBM in the electronic band structure as well in the charge density plots. At the Γ point, such a hybridization is prohibited by the cubic

https://dx.doi.org/10.1021/acs.jpclett.0c01386
J. Phys. Chem. Lett. 2020, 11, 5719−5727

symmetry of the crystal. This is evident in the charge density plot at the Γ point where there is no Pb-s contribution and the VBM solely has Cl/Br-p_z character, which may be arising from a direct hopping between these orbitals. The same analysis was also done for $MAPbBr_3$ (not shown here) and similar results were found. Hence, it can be concluded from the above analysis that the Pb−Cl/Br hybridization (covalency) is highest at the M point, and then it gradually decreases as the Γ point is approached where the covalent character is absent, followed by an increase as one approaches the X point. A schematic representation of bonding−antibonding hybridization between Pb-s and Cl/Br-p is shown in Figure 3d, clearly visualizing the orbital contributions to the valence and conduction bands of hybrid perovskites.

As we have discussed above, the MA^+ orientation has a profound effect on the electronic band structure of hybrid perovskites.[31] For configurations where the MA^+ cations are oriented along the (100) direction and are parallel to each other (ferro-ordering) the potential generated by the MA^+ cations lowers the cubic symmetry even if the unit cell is cubic (model 2) and partially removes the degeneracy at the Γ point associated with nine hybridized Cl-p−Pb-s bands (corresponding to three Cl atoms/unit cell)) even in the absence of spin−orbit coupling (Figure 4a). However, if we use a ferro-ordering of the MA^+ ions along the (110) direction, the bandgap decreases by 0.04 eV and the 9-fold degeneracy is also lifted. These findings clearly indicate that the orientation of the MA^+ ion plays an important role in the electronic band structure by reducing the symmetry.[32−36] Comparison between experimental and theoretical band structures near the Γ point clearly shows a large discrepancy, the latter giving a gap between the top dispersing valence band and the flat band below it, the gap being ∼0.5−1.0 eV. Since in the cubic phase, orientation of the MA^+ cations is dynamically disordered (they are almost freely rotating), one has to sample the band structure for all possible orientations. As discussed earlier, we use model 1 to describe this situation, where we consider only the orientational average of the potential produced by the rotating MA^+ ion, $V_s(r)$, which we represent by replacing the molecular ion by a spherically symmetric Cs^+ ion, which has roughly the same size and same charge.

The resulting band structure of $CsPbCl_3$ is presented in Figure 4b. We find that the nine partially split Cl-p bands of $MAPbCl_3$ at the Γ point (Figure 4a) have nearly 9-fold degenerate Cl-p bands for $CsPbCl_3$ (Figure 4b). The small splitting is caused by spin−orbit interaction. The large gap between the topmost dispersing band and the nearly flat band in Figure 4a is also gone in Figure 4b. The band structure shown in Figure 4b is much closer to the experimental observation, suggesting that model 1 provides a better picture of the orientationally disordered nature of the MA^+ ions.

In order to understand the specific effect of SOC on the band structure we use the two models and focus on the top few (valence) bands only. For model 2 we take the top 2 (valence) bands and for model 1 we take the top 6 (valence) bands. Strong Rashba type spin−orbit split bands are observed at the Γ point for model 2, the orientationally ordered model, when SOC is considered (Figure 5c), while no such effect is observed (Figure 5d) for model 1. More importantly, bands continue to remain doubly degenerate near the M and X symmetry points for both the models.

Our theoretical calculations do not support the giant Rashba splitting in $MAPbBr_3$ reported by Niesner et al.[12] in the

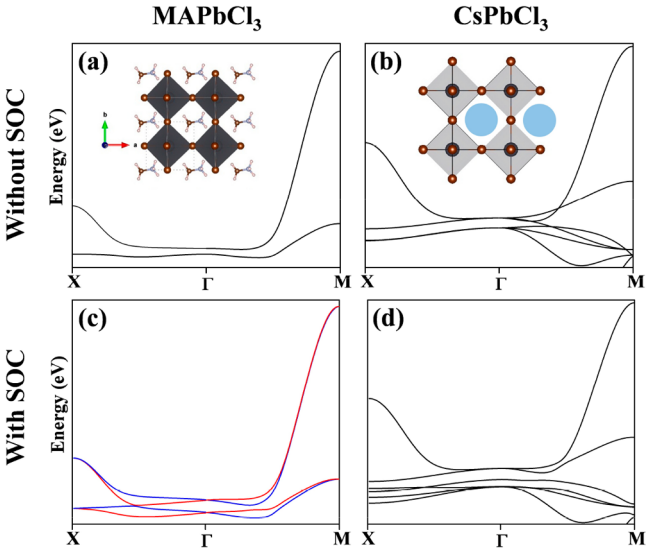


Figure 5. Calculated band structure of $MAPbCl_3$ without (a) and with (c) spin−orbit coupling (SOC), and of $CsPbCl_3$ without (b) and with SOC (d).

disordered cubic phase, where the authors have interpreted the ring-shaped band contours observed near the valence band maxima (i.e., at $\bar{M}$ point) in terms of Rashba splitting. They associate these contours with the splitting of doubly (spin) degenerate bands into two bands shifted with respect to each other in *k* space (Rashba splitting). Their result is an isolated one where a strong Rashba splitting at the $\bar{M}$ point has been claimed. Che et al.[22] also investigated the possibility of the Rashba effect for a 2 × 2 surface reconstructed of $MAPbBr_3$ using first-principles calculations and did find a surface induced Rashba effect. They found a Rashba splitting of much smaller magnitude at the Γ point for specific orientation of the MA^+ molecule, in agreement with our results. Frohna et al.[37] also predicted a Rashba effect in the hybrid perovskite arising from a net electric field from many randomly oriented polar MA^+ ions, which was also supported by McKechnie et al.[38] These results clearly indicate that the spin−orbit coupling induced *k*-dependent valence band splitting arises due to local asymmetry resulting the A-site cation (MA^+).

As ARPES derived intensity maps can provide a direct picture of the *k*-dependence of the electronic bands, we present constant energy plots (iso-energy cuts) derived from 3D band mapping of $MAPbCl_3$ for some selective values of the binding energies in Figure 6a−h. At 2.35 eV below the Fermi edge (Figure 6a), one sees the spectral density in the form of single dot at the $\bar{M}$ symmetry point, which suggests that the top of the valence band projected normal to the (001) surface is at $\bar{M}$. With increasing binding energy, the dot evolves into a closed band contour with the shape of the band contour being decided by the extend of sp hybridization of the Pb-6s and Cl-3p orbitals.[39] At around 3.7 eV binding energy, the top of the valence band at $\bar{X}$ appears in the iso-energy cut. A further increase of binding energy resulted in a cubic (square) band contour around the $\bar{\Gamma}$ point (3.7−3.9 eV) with maximum intensity observed at $\bar{\Gamma}$ at ∼4.5 eV arising from Cl-p_z orbital.

Niesner et al.[12] in their ARPES constant energy maps for the cubic phase of $MAPbBr_3$, taken near the top of the valence band maximum, i.e., at $\bar{M}$, observed a ring-shaped contour, with a minimum spectral intensity at the center. This feature around $\bar{M}$ with a dip at the center was interpreted (as shown in

https://dx.doi.org/10.1021/acs.jpclett.0c01386
J. Phys. Chem. Lett. 2020, 11, 5719−5727

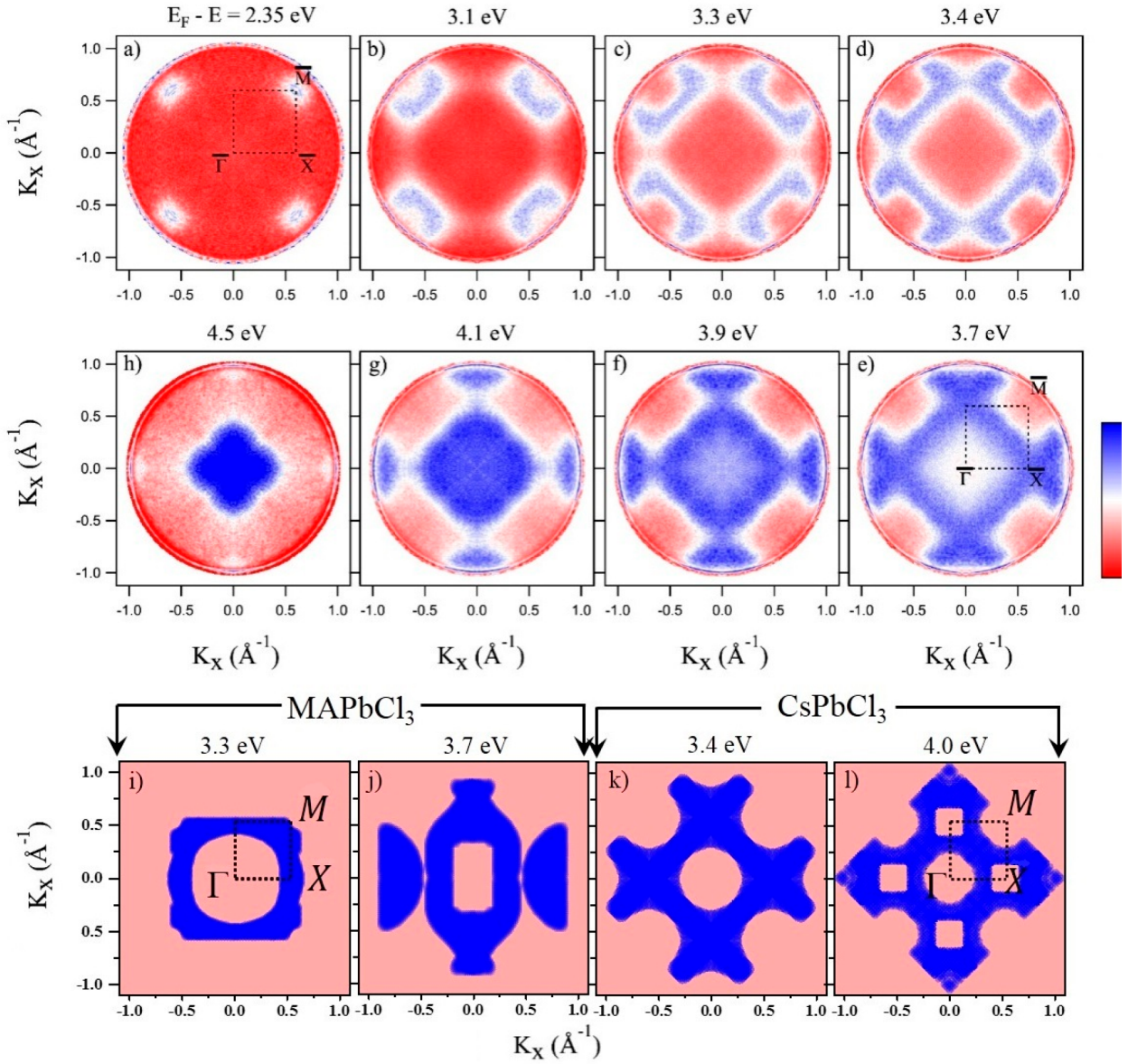


Figure 6. ARPES constant energy contours of the electronic structure in the $\bar{X}$–$\bar{\Gamma}$–$\bar{M}$ plane at different binding energies marked in the figure [(a)–(h)]. Corresponding energy cuts from theoretical data of $MAPbCl_3$, model 2(i,j) and $CsPbCl_3$, model 1 (k,l) are shown.

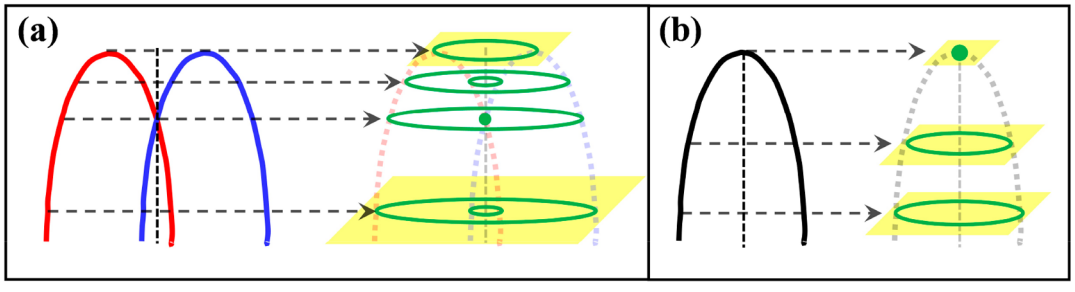


Figure 7. Effect of SOC and the resulting Rashba effect on constant energy contour curves (schematic). (a) In the presence of SOC, the valence band splits into two spin-split bands and corresponding contours at different energies. (b) Without SOC, a doubly spin-degenerate band with a single maximum is expected and corresponding contours at different energies.

the schematics Figure 7a) as the Rashba splitting of the bands. However, within our experimental resolution (for $MAPbCl_3$) we did not observe any drop in the spectral intensity near the top of the valence band maxima (i.e., at $\bar{M}$) and observed a single ring-shaped contour (Figure 6b–d) around $\bar{M}$. This corresponds to a single downward dispersing band (as suggested in schematic Figure 7b) and does not support the idea of Rashba spin-split bands for which one expects to see

https://dx.doi.org/10.1021/acs.jpclett.0c01386
J. Phys. Chem. Lett. 2020, 11, 5719–5727

concentric bands with increasing energy (Figure 7a).[40] Xu et al.[41] also demonstrated that molecular orientations of organic cation influence the fundamental electronic bandgap and the Rashba-type energy band splitting. Assuming a ferro-orientational ordering of the molecule for a cubic unit cell, as we have done, they showed that the Rashba parameter near the valence band maxima is larger in $MAPbX_3$ (1.16 eVÅ) than in $FAPbX_3$ (0.59 eVÅ) or in $EAPbX_3$ (0.84 eVÅ) and that there is no Rashba splitting in $CsPbX_3$, which is consistent with our results.

Although inclusion of spin−orbit coupling in our (and other) theoretical calculation does suggest spin-split bands near the Γ point, in most of these calculations the disordered nature of MA^+ molecular orientation is not taken into account and calculations are performed with a specific orientation of MA^+ molecule. Also, these calculations predict a much smaller band gap than the experimental one.[20,21] Our results (obtained with spherically averaged potential) appear to be more reliable, as they suggest that spin−orbit splitting is not a dominating effect, at least in the cubic phase. While comparing the experimental constant energy contours with the theoretical one (for $MAPbCl_3$, Figure 6i,j), we observe a symmetry lowering (noncubic) in the system. (i) Calculated constant energy contours at 3.3 and 3.7 eV for model 2 are not symmetric about the M point, and (ii) bands about X point are different in the same iso-energy contour. In contrast, model 1 has cubic symmetry, and the constant energy contours are shown in Figure 6k,l. The results of constant energy contours at 3.4 and 4.0 eV match relatively better with the experimental energy contours at 3.3 and 3.9 eV. Thus, a comparison of the valence band dispersion between ferro-ordered model (model 2) and spherically symmetric model (model 1) reveals that the band structure in the organic-molecule orientationally disordered cubic phase may be somewhere between these two extreme limits, but closer to model 1. This can be confirmed by performing coherent-potential approximation in DFT to average over the ensemble of various molecular orientations and provide an average band structure, which is beyond the scope of this paper.

To conclude, we have investigated the electronic structure of $MAPbCl_3$ and $MAPbBr_3$ using photoemission (both angle-integrated and angle-resolved) in the organic molecule orientationally disordered cubic phase and have correlated these results with DFT based theoretical calculations using two different models. Photoemission results suggest strong dispersion of the valence bands, which we find arises from the hybridization between halide Cl/Br-p and Pb-6s (antibonding) orbitals. The two theoretical models used to understand the experimental angle-integrated photoemission results are (1) MA^+ ion is orientationally disordered and the nonspherical part of its potential is small and averages out (we do this by replacing the MA^+ ion by spherically symmetric Cs^+ ion and calculate the band structure of $CsPbCl_3$) and (2) MA^+ ions are orientationally ordered along the (100) direction but constrain the unit cell to retain its cubic structure. Model 2, which breaks the local symmetry caused by molecular orientation, gives a large splitting of the top six p-bands (out of total nine p bands associated with three Cl atoms) near the $\bar{\Gamma}$ point into a group of 2 and 4. This does not agree with the experimental observation. This model also fails to explain the constant energy contours. In contrast, model 1 gives band structure close to the experimental observation where the top six p-bands near the $\bar{\Gamma}$ point are nearly degenerate. Constant energy contour curves obtained with this model also match closely with the experiment. We believe the real situation is closer to model 1 with small MA^+ molecular ion induced nonsphericity correction. Since our theoretical calculations using this model do not give Rashba splitting, experimentally observed small Rashba splitting has to come from nonsphericity corrections caused by local orientational order, albeit random. The effect is, however, weak. However, one can expect to see strong Rashba splitting in the orientationally ordered noncubic phases.

■ ASSOCIATED CONTENT

Supporting Information

The Supporting Information is available free of charge at https://pubs.acs.org/doi/10.1021/acs.jpclett.0c01386.

Preparation procedure of $CH_3NH_3PbX_3$ (X = Br, Cl) single crystals, electronic structure calculations using PAW implementation of DFT within the VASP, atomic positions, "shift and stretch" procedure, crystal structures, X-ray diffraction patterns, photoionization cross-sections, angle-integrated and angle-resolved photoemission spectroscopy (PDF)

■ AUTHOR INFORMATION

Corresponding Author

D. Topwal − *Institute of Physics, Bhubaneswar 751005, Odisha, India; Homi Bhabha National Institute, Training School Complex, Anushakti Nagar, Mumbai 400085, India;* orcid.org/0000-0003-1486-8348; Email: dinesh.topwal@iopb.res.in, dinesh.topwal@gmail.com

Authors

Pronoy Nandi − *Institute of Physics, Bhubaneswar 751005, Odisha, India; Homi Bhabha National Institute, Training School Complex, Anushakti Nagar, Mumbai 400085, India;* orcid.org/0000-0002-3229-5080

S. K. Pandey − *Department of Physics, National Taiwan University, Taipei 10617, Taiwan*

Chandan Giri − *Institute of Physics, Bhubaneswar 751005, Odisha, India*

Vijay Singh − *CEA, LITEN, 38054 Grenoble, France;* orcid.org/0000-0002-4985-2445

L. Petaccia − *ElettraSincrotrone Trieste, I-34149 Trieste, Italy;* orcid.org/0000-0001-8698-1468

U. Manju − *CSIR-Institute of Minerals and Materials Technology, Bhubaneswar 751013, Odisha, India*

Subhendra D. Mahanti − *Institute of Physics, Bhubaneswar 751005, Odisha, India; Department of Physics and Astronomy, Michigan State University, East Lansing, Michigan 48824, United States*

Complete contact information is available at: https://pubs.acs.org/10.1021/acs.jpclett.0c01386

Author Contributions

[▽]P.N. and S.K.P. contributed equally to this work.

Notes

The authors declare no competing financial interest.

■ ACKNOWLEDGMENTS

P.N., C.G., U.M., and D.T. thank the ICTP-Elettra Users' program for providing financial support for performing experiments at the Elettra Synchrotron Light Source, Trieste,

Italy. We acknowledge Elettra Sincrotrone Trieste for providing access to its synchrotron radiation facilities, and we thank S. Thakur, G. Di Santo, and L. Sancin for assistance in using BaDElPh beamline. V.S. acknowledges Ambroise van Roekeghem, CEA-LITEN, France, for his useful discussions. D.T. acknowledges S. R. Barman from the *UGC-DAE Consortium for Scientific Research*, Indore 452001, Madhya Pradesh, India, for preliminary ARPES measurements.

REFERENCES

(1) Babu, R.; Giribabu, L.; Singh, S. P. Recent Advances in Halide-Based Perovskite Crystals and Their Optoelectronic Applications. *Cryst. Growth Des.* **2018**, *18*, 2645−2664.
(2) Nandi, P.; Giri, C.; Bansode, U.; Topwal, D. $CH_3NH_3PbI_3$ Based Solar Cell: Modified by Antisolvent Treatment. *AIP Conf. Proc.* **2016**, *1832*, 080065.
(3) Best Research-Cell Efficiency Chart |Photovoltaic Research| NREL, "https://www.nrel.gov/pv/cell-efficiency.html (accessed: November 2019).
(4) Kumawat, N. K.; Dey, A.; Kumar, A.; Gopinathan, S. P.; Narasimhan, K. L.; Kabra, D. Band gap Tuning of $CH_3NH_3Pb(Br_{1-x}Cl_x)_3$ Hybrid Perovskite for Blue Electroluminescence. *ACS Appl. Mater. Interfaces* **2015**, *7*, 13119−13124.
(5) Nandi, P.; Giri, C.; Swain, D.; Manju, U.; Mahanti, S. D.; Topwal, D. Temperature Dependent Photo-induced Reversible Phase Separation in Mixed Halide Perovskite. *ACS Appl. Energy Mater.* **2018**, *1*, 3807−3814.
(6) Nandi, P.; Giri, C.; Joseph, B.; Rath, S.; Manju, U.; Topwal, D. $CH_3NH_3PbI_3$, A Potential Solar Cell Candidate: Structural and Spectroscopic Investigations. *J. Phys. Chem. A* **2016**, *120*, 9732−9739.
(7) Nandi, P.; Giri, C.; Swain, D.; Manju, U.; Topwal, D. Room Temperature Growth of $CH_3NH_3PbCl_3$ Single Crystals by Solvent Evaporation Method. *CrystEngComm* **2019**, *21*, 656−661.
(8) Wang, C.; Ecker, B. R.; Wei, H.; Huang, J.; Meng, J.-Q.; Gao, Y. Valence Band Dispersion Measurements of Perovskite Single Crystals using Angle-Resolved Photoemission Spectroscopy. *Phys. Chem. Chem. Phys.* **2017**, *19*, 5361−5365.
(9) Endres, J.; Egger, D. A.; Kulbak, M.; Kerner, R. A.; Zhao, L.; Silver, S. H.; Hodes, G.; Rand, B. P.; Cahen, D.; Kronik, L.; Kahn, A. Valence and Conduction Band Densities of States of Metal Halide Perovskites: A Combined Experimental-Theoretical Study. *J. Phys. Chem. Lett.* **2016**, *7*, 2722−2729.
(10) Wang, C.; Liu, X.; Wang, C.; Xiao, Z.; Bi, C.; Shao, Y.; Huang, J.; Gao, Y. Surface Analytical Investigation on Organometal Triiodide Perovskite. *J. Vac. Sci. Technol., B: Nanotechnol. Microelectron.: Mater., Process., Meas., Phenom.* **2015**, *33*, 032401.
(11) Komesu, T.; Huang, X.; Paudel, T. R.; Losovyj, Y. B.; Zhang, X.; Schwier, E. F.; Kojima, Y.; Zheng, M.; Iwasawa, H.; Shimada, K.; Saidaminov, M. I.; Shi, D.; Abdelhady, A. L.; Bakr, O. M.; Dong, S.; Tsymbal, E. Y.; Dowben, P. A. Surface Electronic Structure of Hybrid Organo Lead Bromide Perovskite Single Crystals. *J. Phys. Chem. C* **2016**, *120*, 21710−21715.
(12) Niesner, D.; Wilhelm, M.; Levchuk, I.; Osvet, A.; Shrestha, S.; Batentschuk, M.; Brabec, C.; Fauster, T. Giant Rashba Splitting in $CH_3NH_3PbBr_3$ Organic-Inorganic Perovskite. *Phys. Rev. Lett.* **2016**, *117*, 126401.
(13) Lindblad, R.; Jena, N. R.; Philippe, B.; Oscarsson, J.; Bi, D.; Lindblad, A.; Mandal, S.; Pal, B.; Sarma, D. D.; Karis, O.; Siegbahn, H.; Johansson, E. M. J.; Odelius, M.; Rensmo, H. Electronic Structure of $CH_3NH_3PbX_3$ Perovskites: Dependence on the Halide Moiety. *J. Phys. Chem. C* **2015**, *119*, 1818−1825.
(14) Sarkar, S.; Mahadevan, P. Role of the A-Site Cation in Determining the Properties of the Hybrid Perovskite $CH_3NH_3PbBr_3$. *Phys. Rev. B: Condens. Matter Mater. Phys.* **2017**, *95*, 214118.
(15) Motta, C.; Mellouhi, F. E.; Kais, S.; Tabet, N.; Alharbi, F.; Sanvito, S. Revealing the Role of Organic Cations in Hybrid Halide Perovskite $CH_3NH_3PbI_3$. *Nat. Commun.* **2015**, *6*, 7026.
(16) Fabini, D. H.; Hogan, T.; Evans, H. A.; Stoumpos, C. C.; Kanatzidis, M. G.; Seshadri, R. Dielectric and Thermodynamic Signatures of Low-Temperature Glassy Dynamics in the Hybrid Perovskites $CH_3NH_3PbI_3$ and $HC(NH_2)_2PbI_3$. *J. Phys. Chem. Lett.* **2016**, *7*, 376−381.
(17) Myung, C. W.; Yun, J.; Lee, G.; Kim, K. S. A New Perspective on the Role of A-Site Cations in Perovskite Solar Cells. *Adv. Energy Mater.* **2018**, *8*, 1702898.
(18) Cho, H.; Kim, J. S.; Kim, Y.-H.; Lee, T.-W. Influence of A-Site Cation on the Thermal Stability of Metal Halide Perovskite Polycrystalline Films. *J. Inf. Disp.* **2018**, *19*, 53−60.
(19) Deng, Z.; Wei, F.; Sun, S.; Kieslich, G.; Cheetham, A. K.; Bristowe, P. D. Exploring the Properties of Lead-free Hybrid Double Perovskites using a Combined Computational-Experimental Approach. *J. Mater. Chem. A* **2016**, *4*, 12025−12029.
(20) Even, J.; Pedesseau, L.; Jancu, J. M.; Katan, C. Importance of Spin-Orbit Coupling in Hybrid Organic/Inorganic Perovskites for Photovoltaic Applications. *J. Phys. Chem. Lett.* **2013**, *4*, 2999−3005.
(21) Kepenekian, M.; Robles, R.; Katan, C.; Sapori, D.; Pedesseau, L.; Even, J. Rashba and Dresselhaus Effects in Hybrid Organic-Inorganic Perovskites: From Basics to Devices. *ACS Nano* **2015**, *9*, 11557−11567.
(22) Che, X.; Traore, B.; Katan, C.; Kepenekian, M.; Even, J. Does the Rashba Splitting in $CH_3NH_3PbBr_3$ Arise from 2 × 2 Surface Reconstruction? *Phys. Chem. Chem. Phys.* **2018**, *20*, 9638−9643.
(23) Deshpande, M. S.; Erwin, S. C.; Hong, S.; Mele, E. J. Effective-Medium Theory for the Normal State in Orientationally Disordered Fullerides. *Phys. Rev. Lett.* **1993**, *71*, 2619.
(24) Mahanti, S. D.; Kemeny, G. Effect of Structural Phase Transitions on the Magnetic Properties of Sodium Superoxide. *Solid State Commun.* **1976**, *18*, 159−162.
(25) Nandy, A. K.; Mahadevan, P.; Sen, P.; Sarma, D. D. KO_2: Realization of Orbital Ordering in a *p*-Orbital System. *Phys. Rev. Lett.* **2010**, *105*, 056403.
(26) Riyadi, S.; Zhang, B.; de Groot, R. A.; Caretta, A.; van Loosdrecht, P. H. M.; Palstra, T. T. M.; Blake, G. R. Antiferromagnetic S = 1/2 Spin Chain Driven by *p*-Orbital Ordering in CsO_2. *Phys. Rev. Lett.* **2012**, *108*, 217206.
(27) Mannino, G.; Deretzis, I.; Smecca, E.; La Magna, A.; Alberti, A.; Ceratti, D.; Cahen, D. Temperature-Dependent Optical Band Gap in $CsPbBr_3$, $MAPbBr_3$, and $FAPbBr_3$ Single Crystals. *J. Phys. Chem. Lett.* **2020**, *11*, 2490−2496.
(28) Zhu, H.; Trinh, M. T.; Wang, J.; Fu, Y.; Joshi, P. P.; Miyata, K.; Jin, S.; Zhu, X.-Y. Organic Cations Might Not Be Essential to the Remarkable Properties of Band Edge Carriers in Lead Halide Perovskites. *Adv. Mater.* **2017**, *29*, 1603072.
(29) Kirmani, A. R.; Mansour, A. E.; Saidaminov, M. I.; Cui, X.; Shi, D.; Alofi, A.; Losovyj, Y. B.; Gurung, G.; Paudel, T. R.; Yost, A. J.; Dowben, P. A.; Tsymbal, E. Y.; Amassian, A.; Katsiev, K. Contributions of the Lead-Bromine Weighted Bands to the Occupied Density of States of the Hybrid Tri-Bromide Perovskites. *Appl. Phys. Lett.* **2018**, *113*, 022101.
(30) Boyer-Richard, S.; Katan, C.; Traoré, B.; Scholz, R.; Jancu, J.-M.; Even, J. Symmetry-Based Tight Binding Modeling of Halide Perovskite Semiconductors. *J. Phys. Chem. Lett.* **2016**, *7*, 3833−3840.
(31) Quarti, C.; Mosconi, E.; De Angelis, F. Interplay of Orientational Order and Electronic Structure in Methylammonium Lead Iodide: Implications for Solar Cell Operation. *Chem. Mater.* **2014**, *26*, 6557−6569.
(32) Evans, P. E.; Pink, M.; Zhumekenov, A. A.; Hao, G.; Losovyj, Y.; Bakr, O. M.; Dowben, P. A.; Yost, A. J. Rotationally Free and Rigid Sublattices of the Single Crystal Perovskite $CH_3NH_3PbBr_3$ (001): The Case of the Lattice Polar Liquid. *J. Phys. Chem. C* **2018**, *122*, 25506−25514.
(33) G, S.; Mahale, P.; Kore, B. P.; Mukherjee, S.; Pavan, M. S.; De, C.; Ghara, S.; Sundaresan, A.; Pandey, A.; Guru Row, T. N.; Sarma, D. D. Is CH3NH3PbI3 Polar? *J. Phys. Chem. Lett.* **2016**, *7*, 2412−2419.

https://dx.doi.org/10.1021/acs.jpclett.0c01386
J. Phys. Chem. Lett. 2020, 11, 5719−5727

(34) Govinda, S.; Kore, B. P.; Bokdam, M.; Mahale, P.; Kumar, A.; Pal, S.; Bhattacharyya, B.; Lahnsteiner, J.; Kresse, G.; Franchini, C.; Pandey, A.; Sarma, D. D. Behavior of Methylammonium Dipoles in $MAPbX_3$ (X = Br and I). *J. Phys. Chem. Lett.* **2017**, *8*, 4113−4121.
(35) Govinda, S.; Kore, B. P.; Mahale, P.; Pandey, A.; Sarma, D. D. Can SHG Measurements Determine the Polarity of Hybrid Lead Halide Perovskites? *ACS Energy Lett.* **2018**, *3*, 1887−1891.
(36) Govinda, S.; Kore, B. P.; Swain, D.; Hossain, A.; De, C.; Guru Row, T. N.; Sarma, D. D. Critical Comparison of $FAPbX_3$ and $MAPbX_3$ (X = Br and Cl): How Do They Differ? *J. Phys. Chem. C* **2018**, *122*, 13758−13766.
(37) Frohna, K.; Deshpande, T.; Harter, J.; Peng, W.; Barker, B. A.; Neaton, J. B.; Louie, S. G.; Bakr, O. M.; Hsieh, D.; Bernardi, M. Inversion Symmetry and Bulk Rashba Effect in Methylammonium Lead Iodide Perovskite Single Crystals. *Nat. Commun.* **2018**, *9*, 1829.
(38) McKechnie, S.; Frost, J. M.; Pashov, D.; Azarhoosh, P.; Walsh, A.; van Schilfgaarde, M. Dynamic Symmetry Breaking and Spin Splitting in Metal Halide Perovskites. *Phys. Rev. B: Condens. Matter Mater. Phys.* **2018**, *98*, 085108.
(39) Kronik, L.; Kümmel, S. Gas-Phase Valence-Electron Photoemission Spectroscopy Using Density Functional Theory. *Top. Curr. Chem.* **2014**, *347*, 137−192.
(40) Ast, C. R.; Henk, J.; Ernst, A.; Moreschini, L.; Falub, M. C.; Pacilé, D.; Bruno, P.; Kern, K.; Grioni, M. Giant Spin Splitting through Surface Alloying. *Phys. Rev. Lett.* **2007**, *98*, 186807.
(41) Xu, Q.; Stroppa, A.; Lv, J.; Zhao, X.; Yang, D.; Biswas, K.; Zhang, L. Impact of Organic Molecule Rotation on the Optoelectronic Properties of Hybrid Halide Perovskites. *Phys. Rev. Materials* **2019**, *3*, 125401.

https://dx.doi.org/10.1021/acs.jpclett.0c01386
J. Phys. Chem. Lett. 2020, 11, 5719−5727